JOURNAL OF MATERIALS SCIENCE 27 (1992) 3575–3580

Superplasticity of mullite–zirconia composite

TAKAYUKI NAGANO, HIDEZUMI KATO
Suzuki Motor Corporation, Research and Development Centre, Takatsuka, Hamamatsu 432-91, Japan

FUMIHIRO WAKAI
Government Industrial Research Institute, Nagoya, Ceramic Science Department, 1-1 Hirate-cho, Kita-ku, Nagoya 462, Japan

Tension tests of mullite–zirconia composite were conducted at elevated temperature. A superplastic elongation of 122% could be achieved at an initial strain rate of $2.86 \times 10^{-5} s^{-1}$ at 1550 °C. Strain hardening was observed at strain rates from 1.42×10^{-4} to $2.86 \times 10^{-5} s^{-1}$ at 1550 °C. The addition of zirconia grains to the mullite matrix increased the creep rate of the composite.

1. Introduction

Superplasticity is a phenomenon in which fine-grained polycrystals exhibit exceptionally large elongation at elevated temperatures. When a polycrystal contains a liquid phase at grain boundaries, an elongation larger than 100% can be observed as demonstrated in β-spodumene glass–ceramics [1]. Since the discovery of crystalline superplasticity in Y_2O_3-stabilized tetragonal ZrO_2 polycrystals (Y-TZP) in 1985, the phenomenon in fine-grained polycrystals without a large amount of intergranular liquid phase attracted much interest because of the material's excellent fracture toughness and strength [2]. Superplasticity has so far been reported in such ceramics as ZrO_2–Al_2O_3 composites [3, 4], hydroxyapatite [5] and Si_3N_4–SiC composite [6]. Yoon and Chen [7] observed superplastic deformation of zirconia–mullite composites in which the zirconia is the matrix phase, using compression tests at elevated temperature.

Mullite ($3Al_2O_3 \cdot 2SiO_2$) has been recognized as a high-temperature structural material since Dokko *et al.* [8] demonstrated excellent mechanical properties of polycrystalline mullite which was fabricated from a synthesized powder. High-purity mullite has high creep resistance, low thermal expansion and good chemical stability [9]. Recent advances in powder processing have brought about various high-purity mullite powders which were synthesized by the sol–gel method [10]. The fracture toughness and the strength of the mullite-based composites were improved by dispersing zirconia grains in them [11]. The zirconia dispersion suppresses grain growth of the composite at elevated temperature. The very small grain size of the composite is preferable also for superplastic deformation.

The deformation of mullite and that of mullite–zirconia composite by tensile creep tests and by tension tests is reported.

2. Experimental procedure

2.1. Specimen preparation

The materials which were used in this experiment were high-purity mullite (MP-20, Chichibu Cement Co. Ltd, Kumagaya, Japan) and mullite–zirconia (15 vol % ZrO_2) composite (MZ-15, Chichibu Cement Co.). The mullite was obtained by sintering stoichiometric mullite powder (71.8 wt % Al_2O_3) at 1650 °C for 2 h, and the mullite–zirconia composite was obtained by sintering a mullite–zirconia gel powder at 1610 °C for 3 h. Some properties of the materials were shown in Table I. The particle size distributions of mullite and zirconia grains in mullite–zirconia composite are shown in Figs 1 and 2, respectively. The particle size distribution of mullite grains in mullite is shown in Fig. 3. Comparing Figs 1, 2 and 3, the addition of zirconia grains to mullite suppressed the grain growth of mullite, and the width of particle size distribution became sharp. The average grain size is defined by a linear intercept length as follows:

$$d_{av} = 1.776L \quad (1)$$

where d_{av} is average grain size and L is the linear intercept length. The average grain size of mullite grain and zirconia grains in the composite were 0.88 and 0.59 μm, respectively. The average grain size of mullite was 1.79 μm.

Plates 80 mm × 20 mm × 4 mm were diamond-machined to fabricate the two types of specimen for tension tests and tensile creep tests. The gauge-length area was polished lengthwise using a diamond paste of 1 μm. The tension specimen had a gauge length of 24 mm with a cross-section about 3 mm in diameter. Specimens used in tensile creep tests were designed to have "targets" on both sides of the gauge length portion (25 mm) so that the creep strain could be measured using a non-contacting electro-optical extensometer.

0022–2461

TABLE I Some properties of mullite and mullite–zirconia composite

Material	Al_2O_3 (wt %)	SiO_2 (wt %)	ZrO_2 (wt %)	Density ($g\,cm^{-3}$)	Grain size (μm)	Bending strength (MPa)	Shear modulus (GPa)
Mullite	71.8	28.2	–	3.11	1.79	280	84
Mullite–zirconia	53.7	21.1	25.2	3.55	0.81	410	86

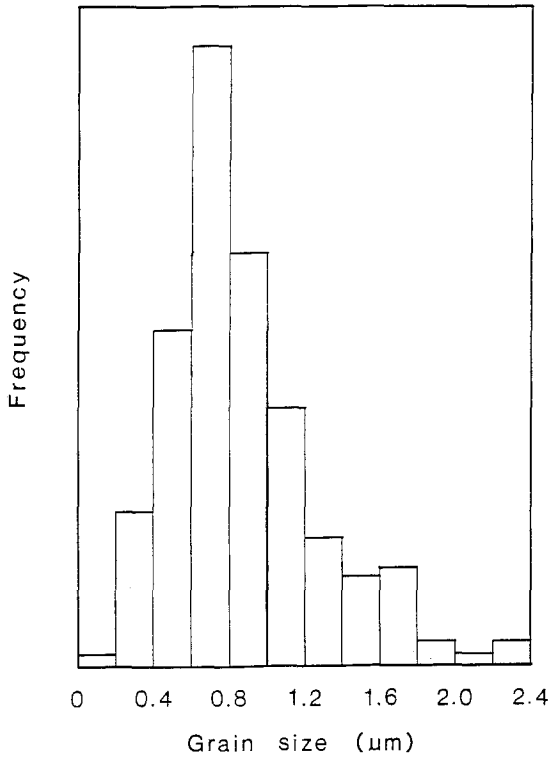

Figure 1 Particle size distribution of mullite grains in mullite–zirconia composite.

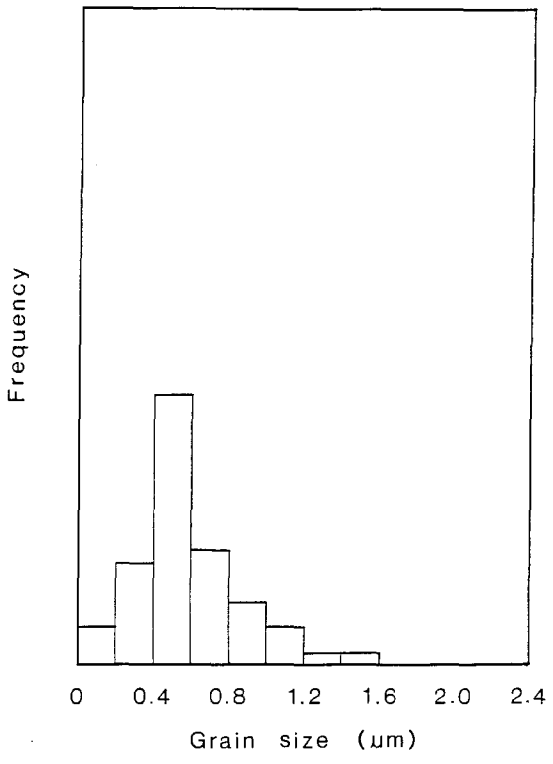

Figure 2 Particle size distribution of zirconia grains in mullite–zirconia composite.

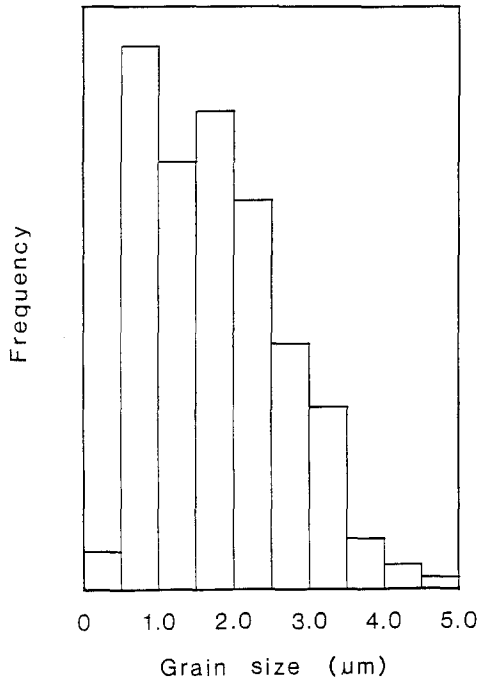

Figure 3 Particle size distribution of mullite.

2.2. Testing methods

Tension tests at constant crosshead speeds were conducted using a universal testing machine after the specimen was heated to 1550 °C. The initial strain rate ranged from 1.42×10^{-4} to $2.86 \times 10^{-5}\,s^{-1}$. Tensile creep tests at constant load were performed in the temperature range 1400–1550 °C and the stress range 10–40 MPa. The gauge portion of deformed specimens and the specimens which were heat-treated under the same conditions as the tension test were observed by scanning electron microscopy to study the microstructural changes.

3. Results

3.1. Mechanical tests

Experimental conditions and the elongation to fracture in tension tests are shown in Table II. A comparison between deformed and undeformed specimens is shown in Fig. 4. An elongation of $> 120\,\%$ was achieved at an initial strain rate of $2.86 \times 10^{-5}\,s^{-1}$ at 1550 °C. The mottled surface of the deformed specimen was caused by reaction of the specimen with the oxidized SiC jig at elevated temperature. The true stress–true strain curves of mullite–zirconia composite in tension tests at 1550 °C is shown in Fig. 5. The true stress–true strain curves were calculated from the load–displacement curves obtained at a constant crosshead speed under the assumption of uniform

TABLE II Summary of tension test data for mullite–zirconia composite

Temperature (°C)	Strain rate (s^{-1})	Elongation (%)
1550	1.42×10^{-4}	22
1550	7.19×10^{-5}	41
1550	3.60×10^{-5}	71
1550	2.86×10^{-5}	122

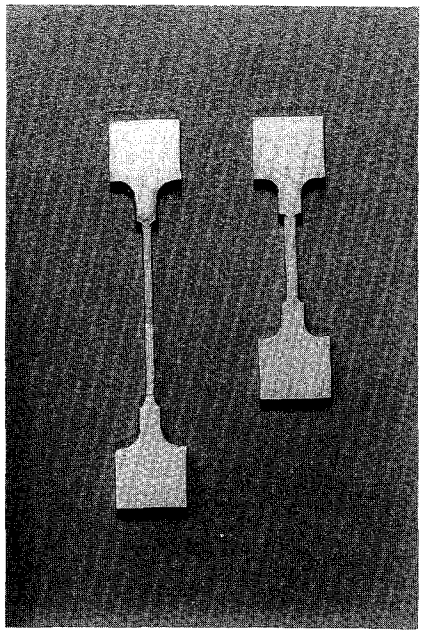

Figure 4 Tensile specimens of mullite–zirconia composite showing superplastic elongation. Initial strain rate = $2.86 \times 10^{-5} s^{-1}$.

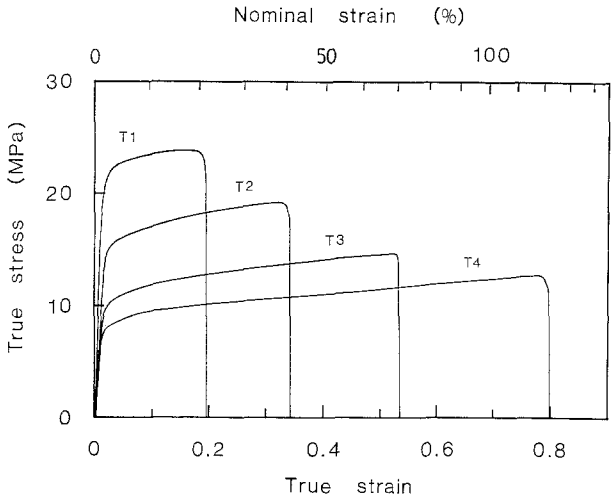

Figure 5 True stress–true strain curves of mullite–zirconia composite in tension tests at 1550 °C. Strain rates (s^{-1}): T1 1.42×10^{-4}, T2 7.19×10^{-5}, T3 3.60×10^{-5}, T4 2.86×10^{-5}.

deformation. The flow stress decreased with the reduction of initial strain rate, and the elongation to fracture increased. Strain hardening was clearly observed at every strain rate used in this experiment.

The creep of ceramics may be expressed by the Dorn equation for a diffusion-controlled process [12]:

$$\dot{\varepsilon} = \frac{AGb}{kT}\left(\frac{b}{d}\right)^{p}\left(\frac{\sigma}{G}\right)^{n} D_0 \exp\left(-\frac{Q}{RT}\right) \quad (2)$$

where G is the shear modulus, b the Burgers vector, k the Boltzmann constant, σ the stress, D_0 a frequency factor, Q the apparent activation energy, R the gas constant, A a constant, n the stress exponent and p the exponent of inverse grain size. The creep rate is dependent on grain size in diffusional creep ($n = 1$, $p = 2$ or 3). When the lattice is the diffusional path (Nabarro–Herring creep), p is 2. When grain boundaries are the diffusional path (Coble creep), p is 3. The creep rate is not dependent on grain size in dislocation creep ($n = 3$–5, $p = 0$). The models proposed for superplasticity consider the major role of grain-boundary sliding. The stress exponent and the exponent of inverse grain size depend on the specific physical model for the rate-controlling process in grain-boundary sliding ($n = 1$–2, $p = 1$–3).

The relationship between flow stress and strain rate which was obtained by tensile creep tests of mullite–zirconia composite is shown in Fig. 6. The stress exponent was calculated from the slope of lines in Fig. 6. The stress exponent of 1.8 at 1400 °C increased with temperature, and became 2.1 at 1550 °C.

The dependence of temperature on strain rate in mullite–zirconia composite is shown in Fig. 7. The apparent activation energy at a stress of 20 MPa is 880 kJ mol^{-1}.

For comparison with the deformation behaviour of mullite–zirconia composite, the results of tensile creep tests on mullite are shown in Fig. 8. The stress exponent of 1.5 at 1400 °C increased with temperature, and became 2.0 at 1550 °C.

The effect of temperature on the strain rate in mullite is shown in Fig. 9. The apparent activation energy at a stress of 20 MPa is 908 kJ mol^{-1}, which is higher than the activation energy of the lattice diffusion coefficient (692 kJ mol^{-1}) [13].

3.2. Microstructural observations

The microstructure of mullite is shown in Fig. 10. A comparison of the microstructures of mullite–zirconia composite for undeformed and deformed specimens is shown in Fig. 11a–c. The microstructures of annealed specimens of mullite–zirconia composite are also shown in Fig. 11d and e. The grey grains are mullite

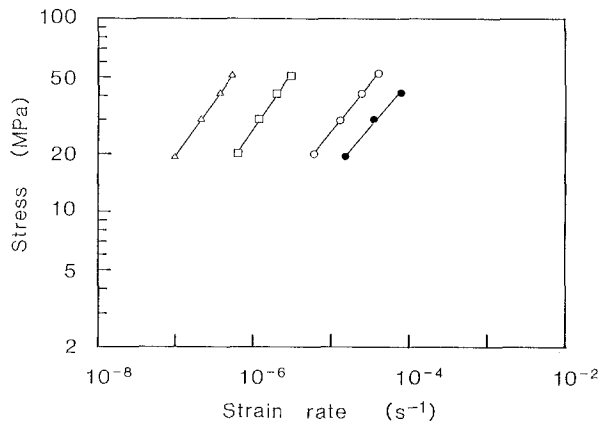

Figure 6 Relationship between flow stress and strain rate in tensile creep tests in mullite–zirconia composite. (△) 1400 °C, $n = 1.8$; (□) 1450 °C, $n = 1.7$; (○) 1500 °C, $n = 2.0$; (●) 1550 °C, $n = 2.1$.

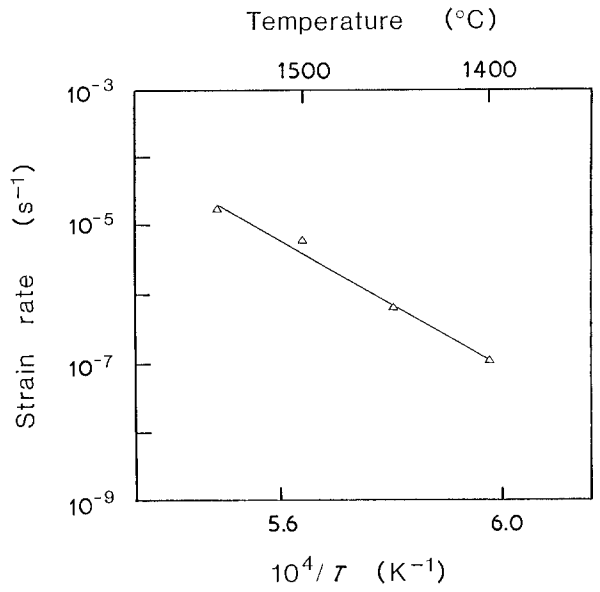

Figure 7 Effect of temperature on strain rate in mullite–zirconia composite. Stress = 20 MPa, Q = 880 kJ mol^{-1}.

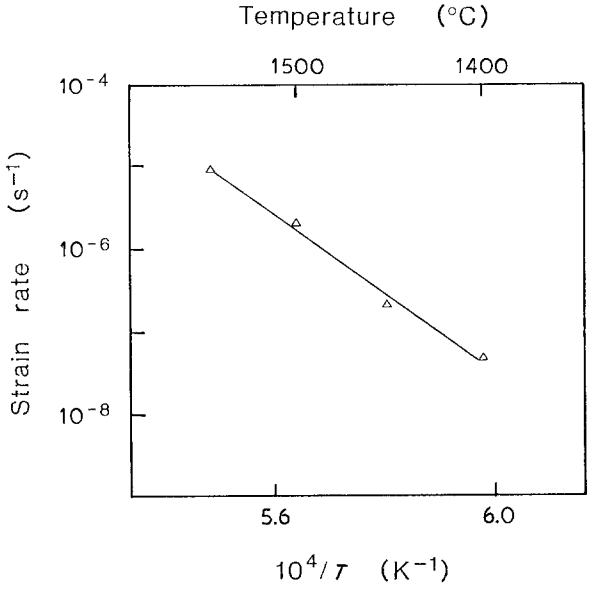

Figure 9 Effect of temperature on strain rate in mullite. Stress = 20 MPa, Q = 908 kJ mol^{-1}.

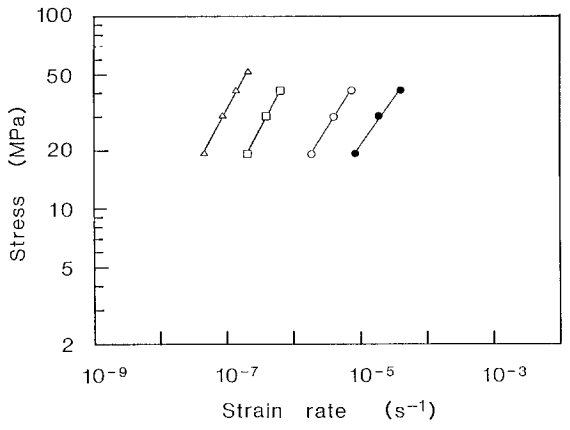

Figure 8 Relationship between flow stress and strain rate in tensile creep tests of mullite. (△) 1400 °C, n = 1.5; (□) 1450 °C, n = 1.5; (○) 1500 °C, n = 1.8; (●) 1550 °C, n = 2.0.

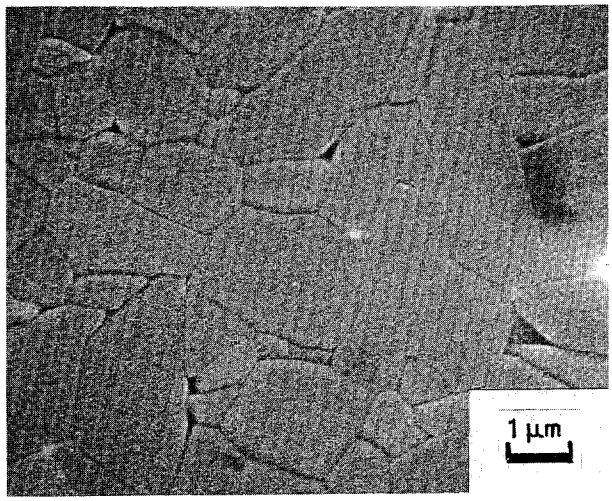

Figure 10 SEM micrograph of as-sintered mullite.

and the white grains are zirconia. Zirconia grains were dispersed among mullite grains in the as-sintered specimen. Mullite grains were elongated and oriented in the tensile direction with increasing deformation. In the elongated specimen, a few instances of cavitation were observed. The grain aspect ratio after a deformation of 122 % was 1.47 in the direction of tensile stress. The ratio of intergranular strain to total strain is therefore calculated to be 32 %. Grain growth and the elongation of mullite grains were also observed in annealed specimens, but the elongated grains did not exhibit preferred orientation.

4. Discussion

We summarize the creep results of mullite first, and then discuss the effect of zirconia dispersion on the creep of mullite–zirconia composite.

Lessing *et al.* [9] conducted creep tests of stoichiometric mullite by four-point bending tests, and reported a stress exponent of 0.95 and an apparent activation energy of 676 kJ mol^{-1} at a stress of 21.9 MPa. They supposed that diffusion was the rate-controlling process of creep. Dokko *et al.* [8] conducted compressive creep tests of mullite and reported a stress exponent of 1, an inverse grain size exponent of 2, and an apparent activation energy of 700 kJ mol^{-1} at a stress of 96.1 MPa. As the apparent activation energy was almost equal to the activation energy of lattice diffusion (692 kJ mol^{-1}) [13], they supposed that the creep mechanism of mullite was Nabarro–Herring creep.

On the other hand, Kumazawa *et al.* [14] conducted tensile creep tests of mullite which was fabricated by sintering a powder synthesized by spray pyrolysis. They reported that the creep rate of mullite was greatly affected by the stoichiometry. The stress exponents of mullite for 68, 71.8 and 78 wt % Al_2O_3 composition were 1.6, 1.6 and 1.8, respectively. Ashizuka *et al.* [15] also conducted four-point bending creep tests of three kinds of mullite which were fabricated from coprecipitated mullite powder. The stress exponents of mullite for 71, 74 and 78 wt % Al_2O_3 were 1.2, 1.4 and 1.1, respectively. The apparent activation energies

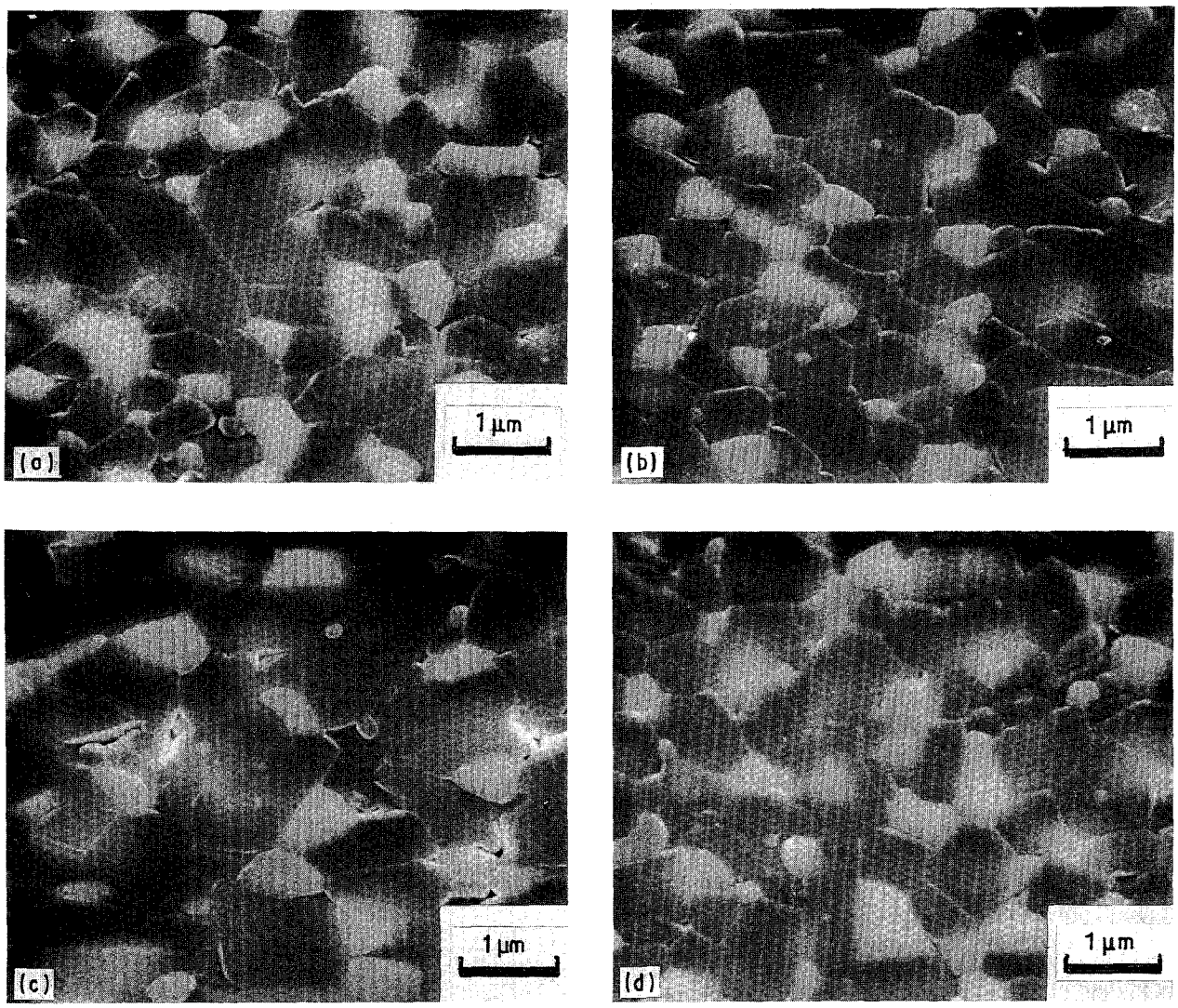

Figure 11 SEM micrographs of (a) as-sintered composite (zirconia is seen as a white phase); (b) after 41% elongation at $\dot{\varepsilon}_0 = 2.86 \times 10^{-5} s^{-1}$ and 1550 °C (tension axis is horizontal), time to failure 246 min; (c) after 122% elongation at $\dot{\varepsilon}_0 = 2.86 \times 10^{-5} s^{-1}$ and 1550 °C (tension axis is horizontal), time to failure 732 min; (d) after annealing for 246 min; (e) after annealing for 732 min.

were 569, 692 and 490 kJ mol^{-1}, respectively, at a stress of 40 MPa. They supposed that the creep mechanism of mullite was grain-boundary sliding by diffusional accommodation. Differences of chemical composition of mullite resulted in differences in the morphology of grains and the constituents of the intergranular phase [14, 16]. The variation in the reported values of stress exponents is supposed to be caused by the variation of microstructure and the difference of experimental conditions. There was good agreement between our results ($n = 1.5$–2.0) and the data of Kumazawa *et al.* [14] ($n = 1.6$–1.8).

As shown in Fig. 6, the stress exponents of mullite–zirconia composite were 1.7 and 2.1 at 1450 and 1550 °C, respectively. The tendency of increasing stress exponent with temperature in mullite–zirconia composite was similar to the tendency in mullite. The apparent activation energy of mullite–zirconia composite at a stress of 20 MPa was 880 kJ mol^{-1}, which was lower than that of mullite.

The exponent of apparent inverse grain size was calculated by assuming that the creep was described by Equation 2, and that the difference of creep rate between mullite and mullite–zirconia composite was caused by only the difference of grain size. However, there are three kinds of grain size for mullite–zirconia composite: (i) the average grain size of the composite, 0.81 μm, (ii) the average grain size of mullite grains in the composite, 0.88 μm, and (iii) the average grain size of zirconia grains in the composite, 0.59 μm. As it is

appropriate to use the average grain size of the composite or that of mullite as the grain size of mullite–zirconia composite, the exponent of inverse grain size (p) is calculated to be about 1. Here, we assumed that the origin of the difference between the strain rate of the composite and that of mullite was the smaller grain size of the composite with zirconia dispersion. However, it is well known that the rate of superplastic deformation in ceramics is significantly changed by a small addition of impurities which segregate at grain boundaries. There is therefore a possibility that the strain rate is changed due to the difference of impurities at grain boundaries between mullite and mullite–zirconia composite. In addition, it is known that the strain rate of a composite is changed by the content of second-phase particles [4]. It is therefore, difficult to specify the deformation mechanism of the composite by these calculations. However, from the experimental results, the deformation of mullite–zirconia composite was expressed as $\dot{\varepsilon} \propto \sigma^2/d$. This equation is similar to the equation for the mechanism of grain-boundary sliding controlled by interfacial reaction which is proposed as a mechanism for superplastic zirconia [17].

5. Conclusion

Tension tests of mullite–zirconia composite were conducted at strain rates from 1.42×10^{-4} to $2.86 \times 10^{-5} s^{-1}$ at 1550 °C, and tensile creep tests of mullite–zirconia composite and mullite were conducted at stresses from 20 to 50 MPa. The results are summarized as follows:

1. Mullite–zirconia composite exhibited a superplastic elongation of 122 % at a strain rate of $2.86 \times 10^{-5} s^{-1}$ at 1550 °C.
2. By the addition of zirconia grains to the mullite matrix, grain growth in sintering was controlled and the creep rate increased.
3. Grain-boundary sliding has an important role in the deformation mechanism of mullite–zirconia composite at elevated temperature.

References

1. J. G. WANG and R. RAJ, *J. Amer. Ceram. Soc.* **67** (1984) 399.
2. F. WAKAI, S. SAKAGUCHI and Y. MATSUNO, *Adv. Ceram. Mater.* **1** (1986) 259.
3. F. WAKAI and H. KATO, *ibid.* **3** (1988) 71.
4. F. WAKAI, Y. KODAMA, S. SAKAGUCHI, N. MURAYAMA, H. KATO and T. NAGANO, in Proceedings of International Meeting on Advanced Materials, Tokyo, June 1988, Vol. 7, "Superplasticity", edited by M. Kobayashi and F. Wakai (Materials Research Society, Pittsburgh, 1988) p. 259.
5. F. WAKAI, Y. KODAMA, S. SAKAGUCHI and T. NONAMI, *J. Amer. Ceram. Soc.* **73** (1990) 457.
6. F. WAKAI, Y. KODAMA, S. SAKAGUCHI, N. MURAYAMA, K. IZAKI and K. NIIHARA, *Nature* **344** (1990) 421.
7. C. K. YOON and I-WEI CHEN, *J. Amer. Ceram. Soc.* **73** (1990) 1555.
8. P. C. DOKKO, J. A. PASK and K. S. MAZDIYASNI, *ibid.* **60** (1977) 150.
9. P. A. LESSING, R. S. GORDON and K. S. MAZDIYASNI, *ibid.* **58** (1975) 149.
10. M. G. M. U. ISMAIL, Z. NAKAI and S. SOMIYA, *ibid.* **70** (1987) C7.
11. *Idem*, in "Advances in Ceramics", Vol. 24, "Science and Technology of Zirconia III" (American Ceramic Society, Pittsburgh, 1988) p. 119.
12. A. K. MUKHEERJEE, J. E. BIRD and J. E. DORN, *Trans. ASM* **62** (1969) 155.
13. I. A. AKSAY and J. A. PASK, *J. Amer. Ceram. Soc.* **58** (1975) 507.
14. T. KUMAZAWA, S. KANZAKI, S. OHTA and H. TABATA, *J. Ceram. Soc. Jpn* **96** (1988) 85.
15. M. ASHIZUWA, T. OKUNO and Y. KUBOTA, *J. Ceram. Soc. Jpn* **97** (1989) 662.
16. Y. KUBOTA and H. TAKAGI, *Proc. Br. Ceram. Soc.* **37** (1986) 179.
17. F. WAKAI, Y. KODAMA and T. NAGANO, *Jap. J. Appli. Phys.* Series 2, (1989) 57.

Received 27 February
and accepted 1 July 1991